Chinese Chemical Letters 33 (2022) 5158–5161

Contents lists available at ScienceDirect

Chinese Chemical Letters

journal homepage: www.elsevier.com/locate/cclet

Surface facets dependent oxygen evolution reaction of single Cu_2O nanoparticles

Yun Shan[1], Xiaoli Deng[1], Xiaoxi Lu, Cong Gao, Yingjian Li, Qianjin Chen*

State Key Laboratory for Modification of Chemical Fibers and Polymer Materials, College of Chemistry, Chemical Engineering and Biotechnology, Donghua University, Shanghai 201620, China

ARTICLE INFO

Article history:
Received 28 December 2021
Revised 2 February 2022
Accepted 3 March 2022
Available online 7 March 2022

Keywords:
Oxygen evolution reaction
Cu_2O nanoparticle
Facets
Scanning electrochemical cell microscopy
Single-particle analysis

ABSTRACT

Understanding and establishing the structure-activity relation of nanoparticles is a prerequisite for rational design of high-performance electrocatalysts. Cu_2O nanoparticles enclosed with different crystal facets, namely, o-Cu_2O NPs with {111} facets, c-Cu_2O NPs with {100} facets are prepared and their electrocatalytic properties for oxygen evolution reaction (OER) in alkaline condition are evaluated at single nanoparticle level with a combination of scanning electrochemical cell microscopy and scanning electron microscopy. It is found that the o-Cu_2O NPs have significantly superior OER electrocatalytic activity compared to c-Cu_2O, which is almost inert. The estimated turnover frequency (TOF) at 1.97 V *vs.* RHE on {111} facet increases from 4 s^{-1} to 115 s^{-1} with the octahedron edge length decreasing from 1.3 μm to 100 nm. Deposition of carbon on c-Cu_2O surface barely promotes the activity, suggesting the inherent poor electric conductivity within the nanocrystal is most likely the reason for low activity. This work provides direct probing to single transition metal oxide crystals with dramatically different activity.

Understanding structure-activity relationship of nanoparticles is of pivotal importance in heterogeneous catalysis. Local structures such as shape, size, and surface facets are well known to have a profound effect on catalytic properties due to different binding energy of key reaction intermediates [1]. Currently, nanoparticle electrocatalytic activities are largely inferred from macroscopic electrochemical [2] or spectroscopic [3] measurement to large ensemble of nanoparticles. However, the structural heterogeneity between individual nanoparticles and integrated additives hold substantial obstacle to build compelling correlation between local structures and intrinsic catalytic activities. Single nanoparticle electrochemistry featuring microscopic electrochemical measurement at single nanoparticles, either by one at a time in collision [4], or spatially resolved in scanning probe electrochemistry [5,6], have revealed unprecedented heterogeneous and dynamic behaviors [6–9]. While the nanoparticle collision electrochemistry allows the estimation of reactivity from transient current signal, the detailed electron transfer is highly related with the dynamic interaction between particle and electrode surface [10,11]. Specifically, scanning electrochemical cell microscopy, a technique using a mobile micro- or nanodroplet at the end of glass pipet scanning across surface, previously developed by Unwin's group [12,13], can visualize nanoscopic electrochemical process as well as physicochemical properties [14,15]. Further coupling SECCM with SEM [16–18], EBSD [19–21], TEM [22], or spectroscopy [23] enables direct and unambiguous correlation between local structure/morphology and electrocatalytic activity. Recently, Choi *et al.* reported that the Au nanocubes have superior hydrogen evolution reaction electrocatalytic activity compared to that of Au octahedrons using single particle SECCM [24].

Cu_2O is one of the most investigated transition metal oxide crystals due to its well-known merits such as low cost and various tailored architectures with easy synthesis [25]. Previous experimental studies have shown high electrocatalytic activity of Cu_2O for OER [26,27]. Most importantly, studies have demonstrated different crystal facets of Cu_2O nanoparticles exhibit distinct catalytic activities and selectivity [28–30]. For examples, using correlated scanning fluorescence X-ray microscopy and TEM, Wu and coworkers directly observed that {110} facet of a single Cu_2O particle is photocatalytically active for CO_2 reduction while the {100} facet is inert [31]. Gao *et al.* elucidated Cu_2O octahedrons (o-Cu_2O) with {111} facets have higher selectivity towards ethylene during CO_2 electroreduction relative to the cubes (c-Cu_2O) with {100} facets [32]. Despite of the fruitful achievement for the facet-dependent of Cu_2O catalysis, direct experimental probing of the activity at microscopic facets and possible effect of the electric contact between Cu_2O nanoparticle and electrode substrate is still lacking.

* Corresponding author.
E-mail address: qianjinchen@dhu.edu.cn (Q. Chen).
[1] These authors contributed equally to this work.

https://doi.org/10.1016/j.cclet.2022.03.010
1001-8417/

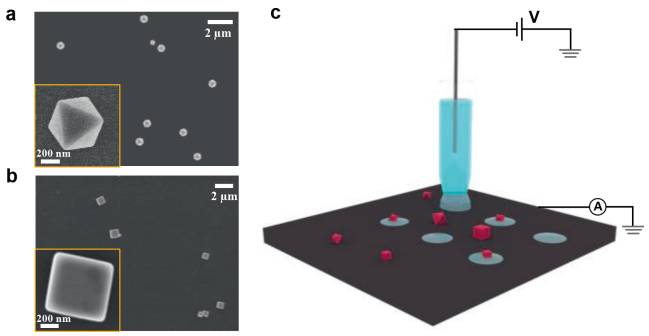

Fig. 1. (a, b) SEM images of synthesized Cu_2O nanoparticles (a: octahedrons, b: cubes) sparsely deposited on glassy carbon. (c) Configuration of SECCM using a single barrel pipet as scanning probe.

Here, we report a microscopic investigation of OER on single Cu_2O nanoparticles with well-defined surface facets ({111} and {100}) using a SECCM technique. Intrinsic electrocatalytic activities of individual nanoparticles are quantitatively assessed and further correlated with surface facets and edge length.

Cu_2O nanoparticles with different surface facets are synthesized in the presence or absence of the selective surface stabilization of polyvinylpyrrolodone (PVP) according to previously reported methods [33]. Scanning electron microscopy (SEM) images show Cu_2O octahedrons (o-Cu_2O) with {111} facets exposed and cubes (c-Cu_2O) with {100} facets exposed with relative uniform sizes (Fig. S1 in Supporting information). XRD patterns show that the as-prepared products are pure Cu_2O crystals and the octahedrons exhibits an obvious increase in diffraction intensity for {111} facet (Fig. S2 in Supporting information). By controlling the hydrothermal reaction temperature, Cu_2O nanocrystals with edge length ranging from 0.1 μm to 1.3 μm were obtained.

The as-synthesized Cu_2O nanoparticles, after been centrifuged for several times to remove free PVP capping agent, were sparsely deposited onto the pre-polished glassy carbon surfaces using a drop-casting method. Upon dried, substrates with Cu_2O nanoparticles were immersed in water for ~2 min to further remove remaining capping agent. Substrate surfaces with no significant agglomeration screened by SEM and optical images (Figs. 1a and b, Fig. S4 in Supporting information) were used to perform SECCM. A single-barrel glass micropipette with a tip opening radius ~1.4 μm (Fig. S5 in Supporting information) and filled with 10 mmol/L KOH aqueous solution was used as the scanning probe (Fig. 1c). A Ag/AgO_x wire was employed as the quasi-reference and counter electrode (QRCE) and its high potential stability during SECCM experiment has been previously demonstrated [17]. The scanning probe was controlled by a piezoelectric motor in the *z* direction and approaches slowly (*e.g.* 1 μm/s) towards the substrate. When the meniscus contacts the substrate, as indicated by an abrupt increase in current passing through the droplet, the piezo would stop and a linear sweep voltammetry (LSV) was performed after a period of 5 s for droplet wetting [19]. The potential *vs.* Ag/AgO_x QRCE in experiments was later converted to the potential to RHE.

Fig. 2a shows a typical SECCM study of oxygen evolution reaction (OER) current at 2.12 V *vs.* RHE at individual o-Cu_2O nanoparticles. As revealed by the correlative SECCM and SEM images, pixels corresponding to Cu_2O nanoparticles shows a higher current than the background. Fig. 2.b shows the array of isolated footprints left from hopping scan and its dimension (~3.0 μm) is in accordance with the pipet diameter (~2.8 μm). Within 169 footprints, 5 spots with one particle were obtained, as outlined by the white circle. For each o-Cu_2O nanoparticle, the LSV in Fig. 2c shows current deviates from the background current on bare carbon spot at approximately 1.82 V *vs.* RHE. From the correlated SEM imaging in Fig. 2d, it is found that an o-Cu_2O nanoparticle with edge length of 483 nm shows an OER current of 0.36 nA at 2.12 V *vs.* RHE while another o-Cu_2O nanoparticle with edge length of 496 nm exhibit a slightly higher current of 0.39 nA. In addition, a smaller o-Cu_2O nanoparticle with edge length of 299 nm exhibits a high OER current of 0.50 nA. Such variations in current indicate the heterogeneity in their catalytic activity of nanoparticles. Close inspection of SEM image shows some particle surface is stained, probably due to the dried KOH solid. Substantial additional electrochemical measurement of single o-Cu_2O nanoparticles are illustrated in Figs. S6 and S7 (Supporting information), constituting the statistic for further activity analysis.

Similar SECCM LSV mapping at 2.12 V *vs.* RHE for single c-Cu_2O nanoparticles with {100} facet and corresponding SEM image of the same area are depicted in Fig. 3. In contrast, the c-Cu_2O nanoparticles exhibit very low OER activity. The measured OER current at 2.12 V on a cube with edge length of 657 nm is 0.06 nA. Additional SECCM images confirm such a low activity of c-Cu_2O nanoparticle for OER (Fig. S8 in Supporting information). We consider three possible explanations for this observation. The first is poor electric contact between the c-Cu_2O nanoparticle and glassy carbon electrode. Previously, Wei *et al*. has pointed out that the electric contact is an important, but often overlooked factor, in single nanoparticle electrochemistry study [34]. They first demonstrated large heterogeneity in ion insertion reaction activity for Prussian blue nanoparticles, and then turned most inactive particles active by depositing an ultrathin platinum or carbon layer onto the sample. We tried a similar carbon deposition procedure using SEM, but found that the OER activity was not significantly promoted (Fig. S9 in Supporting information). Second, possible contribution of remaining polymer ligand on particle surface is excluded since ligand is not involved during the synthesis of c-Cu_2O nanoparticles. Third, previous studies observed facet-dependent conductivity behaviors of Cu_2O nanocrystals and found that the octahedrons are three orders electrically conductive than the cubes [35,36]. We speculate this is the main reason for the observed electrochemical inertness of c-Cu_2O nanoparticles and proper Cu_2O heterostructures [37] and molecular decoration [38] would be favorable to promote charge carrier transport at the c-Cu_2O nanoparticle surface.

Fig. 4a shows the statistical analysis of OER current density at 1.97 V *vs.* RHE for approximately 80 o-Cu_2O and 40 c-Cu_2O nanoparticles, where the current is normalized by particle surface area after background subtraction. To discuss about the intrinsic electrocatalytic activity, the turnover frequency (TOF) is calculated by Eq. 1:

$$\mathrm{TOF} = \frac{i \times N_A}{N \times 4F} \quad (1)$$

where F is the Faraday constant, N_A is the Avogadro constant and N is the number of Cu atoms at corresponding surface of the Cu_2O nanoparticle (3 for {111} facet and 2 for {100} facet, Section S6 in Supporting information). The corresponding TOF is presented in Fig. 4b, ranging from 4 s^{-1} to 115 s^{-1} for octahedrons and 0.05 s^{-1} to 1.5 s^{-1} for cubes. For o-Cu_2O particles, the averaged TOF increases from 10 s^{-1} with edge length of 1.3 μm to 70 s^{-1} with edge length of 100 nm. Such a size dependent OER activity is consistent with results in the literature, where a TOF between 0.1 s^{-1} to 1.2 s^{-1} at 1.92 V *vs.* RHE for $NiFe_2O_4$ superparticles [17], and 531 s^{-1} to 1396 s^{-1} at 1.9 V *vs.* RHE for Co_3O_4 nanocubes was estimated [39], both using the SECCM single particle electrochemistry.

In summary, we reported the utilization of SECCM mapping to study the facet dependent of electrocatalytic oxygen evolution on transition metal oxide nanoparticles at single particle level. It is clearly demonstrated that the o-Cu_2O nanoparticles present at least two orders higher OER activity than the c-Cu_2O, which is

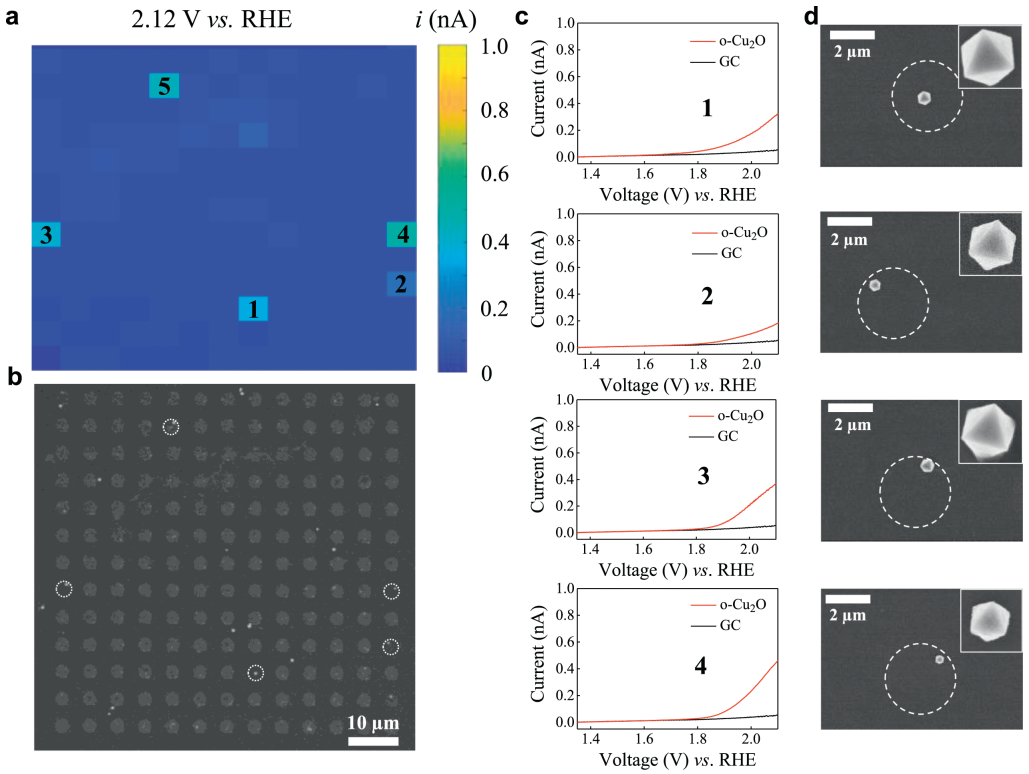

Fig. 2. SECCM study of OER on single o-Cu_2O nanoparticles. (a) Electrochemical current mapping at 2.12 V *vs.* RHE and (b) SEM image of corresponding scanning area with footprints. (c) Typical LSV at 0.5 V/s and (d) localized SEM images of single o-Cu_2O nanoparticles, where catalytic active particles are indicated by white circles. In the experiment, a solution of 10 mmol/L KOH was used as the supporting electrolyte. The spots 1, 2, 3 and 4 contain one octahedron with edge length of 483, 346, 496 and 299 nm, respectively.

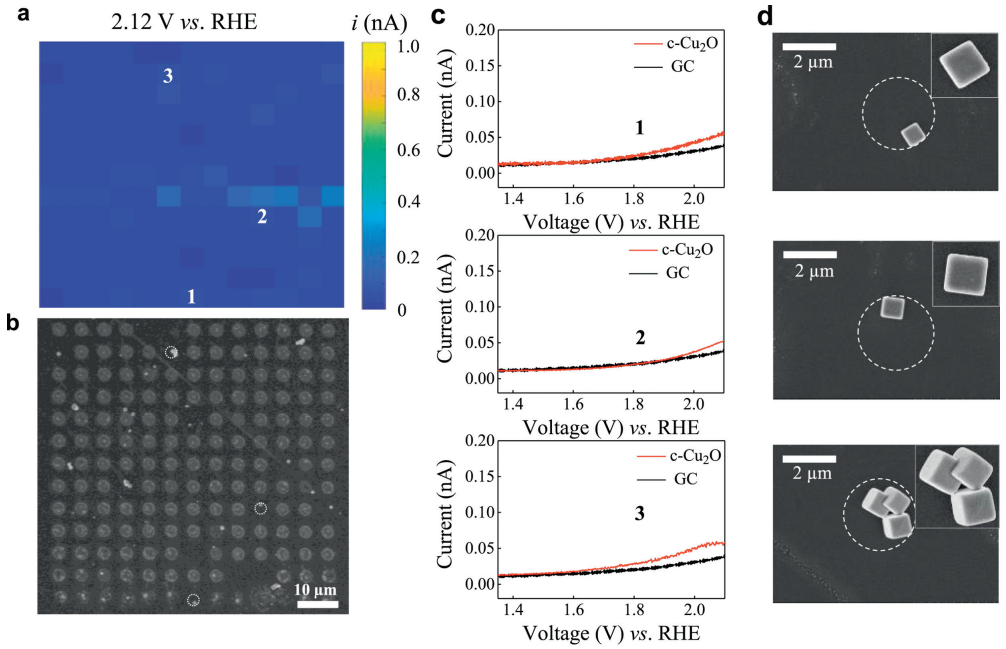

Fig. 3. SECCM study of OER on single c-Cu_2O nanoparticles. (a) Electrochemical current mapping at 2.12 V *vs.* RHE and (b) SEM image of the corresponding scanning area. (c) Typical LSV at 0.5 V/s and (d) localized SEM images of single c-Cu_2O nanoparticles, where catalytic active particles are indicated by white circles. In the experiment, a solution of 10 mmol/L KOH was used as the supporting electrolyte. The spots 1 and 2 contains one cube with edge length of 657, 751 nm, respectively, while the spot 3 has multiple particles, which is not discussed in this study.

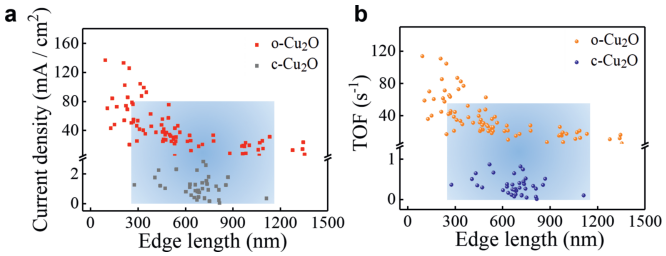

Fig. 4. (a) Current density and (b) calculated TOF of OER at 1.97 V *vs.* RHE at individual o-Cu_2O and c-Cu_2O nanoparticles with different edge length.

almost inert. While the large heterogeneity in electrocatalytic activity of individual particles is clearly demonstrated, the statistical analysis shows the trend that decreasing the particle edge length increases the activity, especially below 600 nm. Our microscopic investigation reveals the intrinsic structure-activity relation of single transition metal oxide nanoparticles. Future works on microscopic SECCM mapping of semiconductor nanoparticles with tunable charge carrier transport properties at surface is highly desirable.

Declaration of competing interest

The authors declare that they have no known competing financial interests or personal relationships that could have appeared to influence the work reported in this paper.

Acknowledgments

We acknowledge the Fundamental Research Funds for the Central Universities (Nos. 2232020A-09, 2232021G-04), Natural Science Foundation of Shanghai (No. 19ZR1470800) and National Natural Science Foundation of China (No. 21804018) and Opening Project of PCOSS from Xiamen University (No. 201906) for financial support. The authors thank Professor Hang Ren for help in SECCM instrumentation, Prof. Patrick Unwin for sharing the software (Warwick Electrochemical Scanning Probe Microscopy).

Supplementary materials

Supplementary material associated with this article can be found, in the online version, at doi:10.1016/j.cclet.2022.03.010.

References

[1] P. Strasser, M. Gliech, S. Kuehl, T. Moeller, Chem. Soc. Rev. 47 (2018) 715–735.
[2] D. Voiry, M. Chhowalla, Y. Gogotsi, et al., ACS Nano 12 (2018) 9635–9638.
[3] Q. Zhang, H. Wang, ACS Catal. 4 (2014) 4027–4033.
[4] S.M. Oja, D.A. Robinson, N.J. Vitti, et al., J. Am. Chem. Soc. 139 (2017) 708–718.
[5] Y. Wang, S.A. Skaanvik, X. Xiong, S. Wang, M. Dong, Matter 4 (2021) 3483–3514.
[6] M.V. Mirkin, T. Sun, Y. Yu, M. Zhou, Acc. Chem. Res. 49 (2016) 2328–2335.
[7] S.E.F. Kleijn, S.C.S. Lai, M.T.M. Koper, P.R. Unwin, Angew. Chem. Int. Ed. 53 (2014) 3558–3586.
[8] F.T. Patrice, K. Qiu, Y.L. Ying, Y.T. Long, Annu. Rev. Anal. Chem. 12 (2019) 347–370.
[9] T.J. Anderson, B. Zhang, Acc. Chem. Res. 49 (2016) 2625–2631.
[10] H. Ma, J.F. Chen, H.F. Wang, et al., Nat. Commun. 11 (2020) 2307.
[11] P.A. Defnet, B. Zhang, J. Am. Chem. Soc. 143 (2021) 16154–16162.
[12] C.G. Williams, M.A. Edwards, A.L. Colley, J.V. Macpherson, P.R. Unwin, Anal. Chem. 81 (2009) 2486–2495.
[13] O.J. Wahab, M. Kang, P.R. Unwin, Curr. Opin. Electrochem. 22 (2020) 120–128.
[14] Y. Liu, C. Jin, Y. Liu, et al., ACS Sens. 6 (2021) 355–363.
[15] Y. Liu, X. Lu, Y. Peng, Q. Chen, Anal. Chem. 93 (2021) 12337–12345.
[16] C.L. Bentley, M. Kang, P.R. Unwin, J. Am. Chem. Soc. 139 (2017) 16813–16821.
[17] X. Lu, M. Li, Y. Peng, et al., J. Am. Chem. Soc. 143 (2021) 16925–16929.
[18] T. Tarnev, H.B. Aiyappa, A. Botz, et al., Angew. Chem. Int. Ed. 58 (2019) 14265–14269.
[19] C.H. Chen, L. Jacobse, K. McKelvey, et al., Anal. Chem. 87 (2015) 5782–5789.
[20] Y. Wang, E. Gordon, H. Ren, Anal. Chem. 92 (2020) 2859–2865.
[21] R.G. Mariano, M. Kang, O.J. Wahab, et al., Nat. Mater. 20 (2021) 1000–1006.
[22] J. Ustarroz, I.M. Ornelas, G. Zhang, et al., ACS Catal. 8 (2018) 6775–6790.
[23] H. Zheng, M. Li, J. Chen, et al., Chin. Chem. Lett. 33 (2022) 1450–1454.
[24] M. Choi, N.P. Siepser, S. Jeong, et al., Nano Lett. 20 (2020) 1233–1239.
[25] S. Sun, X. Zhang, Q. Yang, et al., Prog. Mater. Sci. 96 (2018) 111–173.
[26] T.N. Saada, L. Pang, K.Sravan Kumar, et al., Electrochim. Acta 390 (2021) 138810.
[27] H. Xu, J.X. Feng, Y.X. Tong, G.R. Li, ACS Catal. 7 (2017) 986–991.
[28] Q. Li, P. Xu, B. Zhang, et al., J. Phys. Chem. C 117 (2013) 13872–13878.
[29] F.A.C. Pastrián, A.G.M. da Silva, A.H.B. Dourado, et al., ACS Catal. 8 (2018) 6265–6272.
[30] Y. Shang, L. Guo, Adv. Sci. 2 (2015) 1500140.
[31] Y.A. Wu, I. McNulty, C. Liu, et al., Nat. Energy 4 (2019) 957–968.
[32] Y. Gao, Q. Wu, X. Liang, et al., Adv. Sci. 7 (2020) 1902820.
[33] X. Liang, L. Gao, S. Yang, J. Sun, Adv. Mater. 21 (2009) 2068–2071.
[34] W. Wei, T. Yuan, W. Jiang, et al., J. Am. Chem. Soc. 142 (2020) 14307–14313.
[35] C.H. Kuo, Y.C. Yang, S. Gwo, M.H. Huang, J. Am. Chem. Soc. 133 (2011) 1052–1057.
[36] C.S. Tan, S.C. Hsu, W.H. Ke, L.J. Chen, M.H. Huang, Nano Lett. 15 (2015) 2155–2160.
[37] S.C. Wu, C.S. Tan, M.H. Huang, Adv. Funct. Mater. 27 (2017) 1604635.
[38] T.N. Chen, J.C. Kao, X.Y. Zhong, et al., ACS Cent. Sci. 6 (2020) 984–994.
[39] T. Quast, S. Varhade, S. Saddeler, et al., Angew. Chem. Int. Ed. 60 (2021) 23444–23450.